Annex 9.C.10: Photooxidation Susceptibility of Diluted Bitumen on Water

Photooxidation Susceptibility of Diluted Bitumen on Water

Lindsay J. Hounjet, Rafal Gieleciak, and Heather D. Dettman*
CanmetENERGY – Devon, Natural Resources Canada
Devon, AB, Canada
Heather.Dettman@Canada.ca

Abstract

The persistence of petroleum spilled into aquatic environments is highly dependent on the complex interplay of natural weathering processes, including evaporation, dispersion, biodegradation and photooxidation. While evaporation and biodegradation processes remove non-persistent fractions of crude oil from water relatively quickly, sunlight-induced photooxidation can facilitate slower decomposition of its most persistent components, rendering them more susceptible to the other weathering processes. Although photooxidation of crude oil has been the subject of many investigations, the process complexity has hindered detailed analyses of the relative susceptibility of different types of chemical species in the oil. Moreover, reports on the photooxidation chemistry of heavy oils, such as diluted bitumen, are scant.

In this work, a simple mixture of nine model compounds representing chemically distinct components of crude oil was applied to the surface of water and exposed to simulated sunlight equivalent to 2, 4, and 6 month periods on Canada's west coast. Detailed chemical analyses of the weathered model mixture were then performed to enable comparisons of the relative photooxidation susceptibilities, reactivity patterns, and degradation products of the different chemical constituents. The effects of irradiation and evaporation processes were considered independently in terms of their contributions to the removal of the chemical components from the water. Similar photooxidation experiments were then conducted using subfractions of diluted bitumen to illustrate the presence of the same decomposition pathways. This study provides chemical information for how photooxidation can facilitate removal of persistent petroleum from water environments.

1 Introduction

Diluted bitumen (DB) from Alberta's oil sands has been transported within Canada for over ten years. With an expected increase in production and transportation, concerns have been raised over how DB may differ from conventional crude oil when spilled into sensitive water environments (Markusoff, 2017). In response to these concerns, several comprehensive reports on the fate and behaviour of DB and other crude oils in water environments have been published (Environment Canada et al., 2013; Witt O'Brien et al., 2013; Lee, K. et al., 2015; NAS, 2016). Recent experimental investigations of DB's interactions with water have examined the effects of chemical dispersants and/or mineral fines on surface spills (King et al., 2015; O'Laughlin et al., 2016), and the effects of chemical pretreatments (Hounjet and Dettman, 2016). The physicochemical properties of DB as they compare to conventional crude oil have been also reported (Zhou et al. 2015). However, less is understood about how different natural weathering processes, including evaporation, dispersion, sedimentation, biodegradation and photooxidation, affect the behaviour of DB in water environments (Environment Canada et al., 2013). From among these processes, biodegradation and photooxidation operate synergistically to effect chemical transformations of spilled oil (Dutta et al., 2000; Maki et al., 2001; Lee, 2003). While

Hounjet, L.J., R. Gieleciak, and H.D. Dettman, Photooxidation Susceptibility of Diluted Bitumen on Water, Proceedings of the Fortieth AMOP Technical Seminar, Environment and Climate Change Canada, Ottawa, ON, pp. 860-884, 2017.

biodegradation acts relatively quickly on the lighter components of crude oil, photooxidation facilitates slower decomposition of the heavier, more persistent components, rendering them prone to other weathering processes (Garrett, 1998). A recent report from the National Academy of Sciences stated that: "photooxidation of diluted bitumen in the environment has hardly been studied and its role in the weathering of spilled diluted bitumen is not well understood" (Committee on the Effects of Diluted Bitumen on the Environment, 2016).

It has been observed that sunlight-induced oxidation of crude oil results in the formation of a dense crust on the exposed surface (Bobra and Tennyson, 1989). In an earlier monograph from the National Academy of Sciences, photooxidation was identified as one of five major mechanisms responsible for the sinking of heavy oil (NAS, 1999). However, it has also been reported that the buoyancy behaviour of DB in marine conditions depends more strongly on the presence of medium-to-fine sediment in the water column, and that evaporative and photooxidative weathering in combination resulted in products that were buoyant in marine conditions (Environment Canada et al., 2013). It has also been found that the effect of photooxidation on the chemical composition of heavy oil released from the 2002 Prestige spill were "not significant at sea" during the year following the spill (Díez et al., 2007).

DB is a complex mixture of innumerable chemically distinct hydrocarbons, which makes it difficult to determine how photooxidation processes affect each of its molecular components. Previous work has shown that saturated compounds resist photooxidation while aromatic compounds are more susceptible, particularly those that are highly substituted or have high molecular weights (Garrett, 1998). Although numerous reports on photooxidation of individual petroleum model compounds in solution phase are available, little is known about the relative photooxidation rates of different hydrocarbon components within crude oils and the chemical identities of photooxidized intermediates in water environments (Ehrhardt et al., 1997). From environmental and toxicological standpoints, important questions pertaining to the behaviour and fate of spilled DB include: "how do different chemical components of DB compare in terms of their photooxidation susceptibility?" and "what are the chemical compounds produced?"

The chemical mechanism of petroleum photooxidation involves initial conversion of aromatic and aliphatic hydrocarbons to the corresponding alcohols. Figure 1 shows how further oxidation of an aromatic alcohol derived from toluene is dearomatized to a reactive organoperoxyl radical intermediate which, after rearrangement, undergoes oxidative ring-opening and cleavage of the remaining bonds between carbon atoms, ultimately producing CO_2 and water (Forstner, 1997; Sato, 2007).

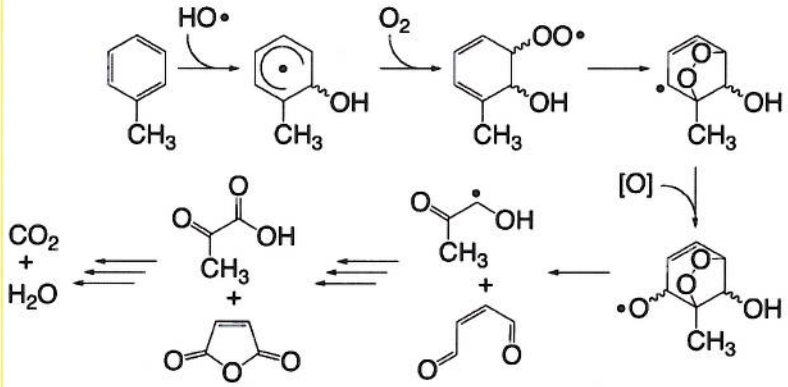

Figure 1. One among many possible degradation pathways for complete photooxidation of toluene

In the case of aliphatic alcohols, photooxidation instead proceeds by hydride ion abstraction from hydroxyl groups to generate aldehyde and ketone intermediates that are attacked by oxygen to generate carboxylic acids that undergo decarboxylation, which shortens the aliphatic chain and produces CO_2 and water. As photooxidation proceeds, the incorporation of oxygen into molecular structures increases both their water-solubility and surfactant functionality, which in turn increases their rates of bio-degradation and bio-mineralization.

As there are yet no standardized or widely accepted methods for evaluating photooxidation of crude oils (Environment Canada, 2013), an array of irradiation and analysis techniques have been applied to study their photo-chemistry (Shankar et al., 2015). Common to many studies is the use of gas chromatography (GC) coupled with either mass spectrometry (MS) or flame ionization detection (FID) techniques as a means of characterizing molecular composition (i.e., Minero et al., 1997; King et al., 2014; Gong et al., 2014). However, GC-based methods are limited to analysis of only the lighter fraction of a crude that evaporates without undergoing thermal decomposition (i.e., boiling point < *ca.* 350 °C at ambient pressure). Despite this drawback, the use of GC to determine boiling point distributions of crude oils via high temperature simulated distillation (HTSD) is well-established; rather than providing data on chemical composition, HTSD instead allows for approximation of the proportions of a sample that can and cannot be analyzed. Thus, knowledge of boiling point distribution, such as may be obtained by HTSD, is imperative for truly quantitative chemical analysis of crude oils by GC.

Nuclear magnetic resonance (NMR) spectroscopy is a powerful, non-destructive technique that enables quantification of various hydrocarbon types within whole crudes (Yang, 2015). To date, however, this technique has been underutilized for the study of crude oil photooxidation chemistry (Maki, 2001). NMR analyses can also be used to quantify individual compounds constituting relatively simple mixtures so long as each contains a spectroscopically distinguishable carbon type. In particular, $^{13}C\{^{1}H\}$ NMR spectroscopy offers excellent resolution of signals attributable to chemically distinct ^{13}C nuclei and, given appropriate data acquisition parameters, can be used to quantify chemically distinguishable sample components. By combining NMR data with those acquired by Fourier transform infrared (FTIR) spectroscopy, GC (HTSD), and elemental analysis, a much more complete understanding of sample composition can be achieved.

In the present experimental work, the relative photooxidation susceptibility and fate of chemically distinct components of petroleum were evaluated. A series of model compounds representing common petroleum hydrocarbon types was selected and blended to form a model mixture. The mixture was then applied to the surface of water and irradiated. After irradiation, the organic-extractable fraction was isolated and characterized to determine the relative photooxidation susceptibilities of these components. The identities of major photooxidation products were also determined. This approach was then applied to DB as well as its saturates and aromatics subfractions.

2 Experimental

2.1 Materials

The model compounds listed in Table 1, as well as hexamethyldisiloxane (HMDSO; ≥ 99.5 %), deuterochloroform ($CDCl_3$; 99.8 atom % D), dichloromethane (CH_2Cl_2; ≥ 99.8 %), toluene (99.8 %), sodium chloride (NaCl; ≥ 99 %), cyclohexanebutyric acid (CHBA; 99 %), and dimethyl sulfoxide (DMSO; ≥ 99 %) were purchased from Sigma-Aldrich and used as received. When not in use, all compounds and mixtures were kept in the dark at –20 °C. The model

compounds listed in Table 1 were added in approximately equimolar proportions (5 mmol each) to the same 20 mL scintillation vial on an analytical balance. The mixture was then homogenized to produce a moderately viscous, orange-coloured solution. Diluted bitumen (DB) was obtained from the Canadian Association for Petroleum Producers, and a sample was distilled to remove the fraction boiling below 204 °C. A sample of this devolatilized DB was then separated into its saturates, aromatics, resins and asphaltenes (SARA) subfractions using a modified variant of American Society for Testing and Materials (ASTM International, West Conshohocken, PA, 2007, www.astm.org) protocol D2007. A sample of DB, with its light ends removed on a rotary evaporator as described below in section 2.3, referred to as DB > 200 °C, was also prepared for comparison with other samples subjected to rotary evaporation as performed during the organic extraction procedure.

Table 1. Model compounds constituting the original mixture

#	Name	F. W. (g/mol)	Mass Used (g)	Purity (%)	BP (°C)[a]
1	Dibenzothiophene	184.26	0.9398	98	333
2	Cyclohexylbenzene	160.26	0.8181	98	240
3	*trans*-Decalin	138.25	0.7061	99.5	187
4	1-Ethyl-2-methylindole	159.23	0.8214	97	267
5	1-Phenyloctane	190.32	0.9599	99	263
6	Benzyl sulfide	214.33	1.0723	98	306[b]
7	*n*-Dodecyl sulfide	370.72	1.9933	93	455[c]
8	Tetralin	132.20	0.6723	99	207
9	1-Methylnaphthalene	142.20	0.7481	95	243

[a] Boiling point at 760 mmHg. [b] Calculated from BP of 131 °C at 2 mmHg. [c] Calculated from BP of 260 °C at 4 mmHg.

2.2 Irradiation

A 1.00 g mass of oil (model mixture, DB or subfraction) was added to the surface of 30.0 mL of deionized water in a 60 mL vial on a balance, and the exact initial mass (m_I) of oil was recorded. The uncapped vial was brought into a fume hood and placed into a jacketed cooling bath maintained at 10.0–11.0 °C. A horizontally collimated beam of light produced by a Newport® Xe arc lamp source operating at 350 W was passed through a 5 cm-long deionized water filter and an Air Mass 1.5 global filter to approximate the solar spectrum (Shankar, 2015). The beam was then turned 90° using a full spectrum mirror so that it projected vertically downward onto the centre of the oil's surface. The incident radiative power at the surface was measured as 0.25 W using a power meter with a 6.0 mm diameter aperture, corresponding to an irradiance of 2.3 kW/m^2 (about twice as intense as maximum solar irradiance at Earth's surface). In the interest of time, irradiation was performed continuously for a period of 0, 4, 8, or 12 days, rather than simulating daily cycles of varying solar intensity. Taken together, these modifications resulted in a 16-fold amplification of photo-exposure relative to the annually averaged solar irradiance measured at Vancouver, Canada (calculated as 0.14 kW/m^2 using Solar Electricity Handbook, 2017). Thus, 4-, 8-, and 12-day-long irradiation periods with simulated sunlight are approximately equivalent in terms of photo-exposure to 2, 4 and 6 months of natural sunlight at this location.

2.3 Extraction

Following irradiation, evaporation of water from the vial was found to be negligible in all cases, and the contents of the vial were poured through a wide-mouth funnel into a 250 mL separatory funnel containing 3.00 g of sodium chloride (NaCl, used to facilitate the separation). The vial was washed with a 30 mL aliquot of dichloromethane (CH_2Cl_2) followed by a 90 mL aliquot of deionized water. The washings were transferred to the separatory funnel, which was then sealed with a stopper, agitated vigorously for 1 min, and left undisturbed for 5 min to allow for separation of the aqueous and organic layers. The underlying organic layer was drained into a pre-weighed 125 mL jar. Additional aliquots of CH_2Cl_2 (2 x 30 mL) were used to wash the vial and the aqueous phase until each appeared colourless. These washings were combined with the organic phase in the jar. The aqueous phase was discarded. The jar was left open under a brisk stream of N_2 at 40 °C in an evaporation chamber for 3 h. The jar was then reweighed and the total mass recovered (m_R) was recorded. The solid residue remaining in the jar was homogenized with a spatula prior to sample analysis. It is important to point out that this extraction procedure resulted in a single recovered product that contained components of the irradiated oil distributed among both the floating slick and the water, and that the distribution of components among these two phases was not discerned.

2.4 Analysis

NMR spectroscopy. Samples were prepared by adding a mass of analyte ($m_A \sim 15$ mg for ^1H, ~ 100 mg for ^{13}C) into a vial on an analytical balance, followed by a known amount of internal standard, HMDSO ($m_H \sim 6.0$ mg for ^1H, ~ 40.0 mg for ^{13}C). Deuterochloroform ($CDCl_3$, 650 µL) was then added to dissolve the mixture. The solution was transferred to an NMR tube and analyzed. ^1H and $^{13}C\{^1H\}$ NMR spectra were obtained using a Varian Unity INOVA AS600 spectrometer operating at 599.734 and 150.817 MHz, respectively. Proton data were acquired using a 3.0 s acquisition time, a 4.0 s recycle delay, a 20 kHz sweep width, and a 30° pulse flip angle. The proton spectra consisted of 128 scans and were referenced to residual $CHCl_3$ at 7.24 ppm. A line broadening of 0.3 Hz was used for signal-to-noise improvement. Quantitative carbon data were acquired using a 1.0 s acquisition time, a 15.0 s recycle delay, a 36166 Hz sweep width, and a 30° pulse flip angle. The carbon spectra consisted of 3600 scans and were referenced to the $CDCl_3$ resonance at δ_C 77 ppm. Reverse-gated waltz decoupling was used to prevent nuclear Overhauser effect enhancements. A line broadening frequency of 2.0 Hz was used for the model compounds for signal-to-noise improvement while linebroadening of 5 Hz was applied to the DB samples.

The $^{13}C\{^1H\}$ NMR spectrum of the original model mixture was compared to those obtained for the individual model compounds to identify the most clearly discernible signal resulting from each in the mixture. As shown in Table 2, a range of chemical shifts was defined for each signal chosen to represent a model compound, over which the integrated signal intensity was used to quantify each component relative to the internal standard, HMDSO signal (δ_C 1.97 ppm).

Table 2. $^{13}C\{^{1}H\}$ NMR integral regions used to quantify compounds in model mixtures

Compound		δ_C (ppm)	
#	Name	Start	End
1	Dibenzothiophene	122.97	122.76
2	Cyclohexylbenzene	44.90	44.58
3	*trans*-Decalin	43.80	43.50
4	1-Ethyl-2-methylindole	37.84	37.66
5	1-Phenyloctane	36.24	36.00
6	Benzyl sulfide	138.35	138.18
7	*n*-Dodecyl sulfide	32.60	32.16
8	Tetralin	23.50	23.16
9	1-Methylnaphthalene	19.60	19.36
	HMDSO	2.40	1.60

Data processing of the ^{13}C and ^{1}H NMR spectra collected for DB samples using the CanmetENERGY carbon type analysis method utilized integral data from both ^{13}C and ^{1}H NMR spectra. The integral regions used and the calculations performed were based on the method published previously (Japanwala et al., 2002) with enhancements. The cluster-size calculations of aromatic and cycloparaffinic rings were based on the method described previously (Solum et al., 1989). Integral values from proton and carbon spectra were used to calculate the molar proportions of various carbon types. To check the fit of the data, the mole % carbon was converted to weight % carbon where the total was set to the values measured by elemental analyses. The NMR data were then used to calculate the hydrogen content (weight %). The difference between the elemental- and NMR-determined hydrogen contents was usually within 1 weight %.

Elemental Analysis. Carbon, hydrogen, nitrogen, and sulfur (CHNS) contents of samples were measured by ASTM method D5291 using an Elementar Variomicrocube Analyzer. Oxygen (O) contents were measured using the same instrument following the manufacturer's recommended method. Total CHNSO proportions were then normalized to 100 % of the sample's mass.

FTIR Analysis. Samples were prepared by adding a mass of analyte ($m_A \sim 50.0$ mg) to a vial on an analytical balance. Dichloromethane (700 µL) was added to the vial to dissolve the analyte. The resulting solution was transferred to a KBr cell and the sample was analyzed using a Bruker Tensor 27 spectrometer. FTIR spectra consisted of an average of 5 repetitions of 32 scans between 4000 and 400 cm^{-1} with the spectrum of the sample divided by that of the solvent background. The resulting spectra were then normalized with respect to the corresponding mass of analyte. Calibration curves were developed by obtaining FTIR spectra of solutions with a range of concentrations of cyclohexanebutyric acid (CHBA) in toluene, and plotting their concentration against the intensity of the carbonyl (C=O) stretching band centred at $\tilde{\nu} = 1709$ cm^{-1}.

GC Analysis. Model oil samples were analyzed for boiling point distribution via high-temperature simulated distillation (HTSD) by modified ASTM method D7169 in CH_2Cl_2 solvent using an Agilent Technologies 6890 gas chromatograph and Analytical Solutions software. HTSD analyses of the DB samples were run using the same instrument and software by the usual ASTM method D7169 (in carbon disulfide). For model oil component identification purposes,

two-dimensional gas chromatography time-of-flight mass spectrometry (GC×GC-TOF-MS) was performed on a LECO Pegasus 4D system (Leco Instruments, Mississauga, ON, Canada) equipped with an Agilent 7890 gas chromatograph (Agilent Technologies, Mississauga, ON, Canada) and a Leco dual-stage, quad-jet thermal cryogen-free modulator and secondary oven. The columns used for the analysis were as follows: primary column, Agilent VF-5ht (30 m × 0.25 mm × 0.1 μm); secondary column, SGE Analytical Science BPX-50 (1.2 m × 0.1 mm × 0.1 μm). The primary oven temperature was initially held at 50 °C for 2 min and then increased at a rate of 5 °C min^{-1} up to 340 °C, where it was held for 2 min. The secondary oven temperature programming tracked the primary program with a +10 °C offset. Method-specific parameters were as follows: inlet temperature, 340 °C; sample injection volume, 0.2 µL; split ratio, 5 : 1; carrier gas, helium (grade 5.0, Air Liquide); modulator temperature, +55 °C offset from the primary oven; and modulation period, 8 s. Data were acquired from 45-500 u with an acquisition rate at 100 spectra/second. The transfer line temperature was 350 °C and the ion source temperature was set to 200 °C.

3 Results

3.1 Photooxidation of Model Mixture

The original mixture consisted of the model compounds depicted in Figure 2: dibenzothiophene (**1**), cyclohexylbenzene (**2**), *trans*-decalin (**3**), 1-ethyl-2-methylindole (**4**), 1-phenyloctane (**5**), benzyl sulfide (**6**), *n*-dodecyl sulfide (**7**), tetralin (**8**), and 1-methylnaphthalene (**9**).

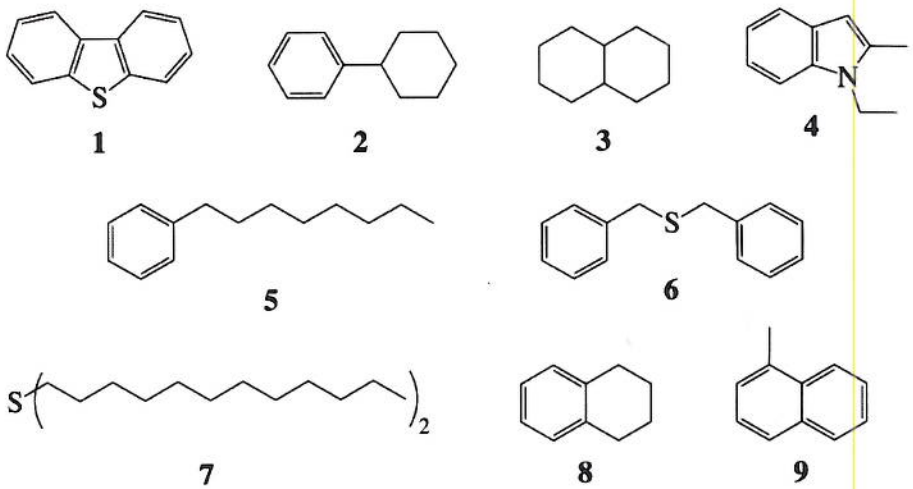

Figure 2. Model compounds constituting the original mixture

These compounds, which represent common hydrocarbon types present in petroleum products such as DB, were selected such that their combination would produce a homogeneous liquid solution with a boiling range of *ca.* 200–500 °C. The decision to omit linear and branched alkanes from the mixture was based on their lack of discernable signals in NMR spectra in addition to the well-known resistance of such compounds to photooxidation (Garrett, 1998). The original mixture was a homogeneous, moderately viscous, transparent, orange-coloured solution. With the exception of 1-ethyl-2-methylindole (**4**), which appeared as a bright-orange liquid, none of the mixture's individual components had a noticeable colour. When applied to the surface of

fresh (deionized) water in a vial, the original mixture evenly covered the surface to form a layer ~2 mm thick.

After 3 h of irradiation, the mixture underwent a noticeable colour change from orange to burgundy, and portions of the slick began to solidify. The rapid onset of solidification appeared to be due to the reduced temperature (10–11 °C) of the system, combined with the evident photochemical (colour) change, and possible evaporation of the most volatile components. After 4 d of irradiation, a continuous sheet of solid material had formed and the underlying aqueous phase took on a pink hue. After 12 d of irradiation, the floating sheet of material had become nearly black while the aqueous phase had become red in colour and nearly opaque. After the irradiation period, the mixture was extracted with CH_2Cl_2 to produce a nearly colourless aqueous phase atop the underlying burgundy-coloured organic phase. Isolation and removal of the solvent from the organic phase produced a dark, adhesive, solid residue. Analogous samples irradiated for 4 and 8 d were also isolated, as was a non-irradiated control mixture, obtained as a viscous, pink-coloured liquid. The masses of samples recovered by organic extraction were then used to calculate the mass recoveries of each sample as reported in Table 3. Oil components distributed among the floating slick and water phases were combined during extraction to eliminate the effect of oil/water partitioning on mass recovery.

Table 3. Recoveries of model mixtures after irradiation and/or extraction

Irradiation Time (d)	**0**	**4**	**8**	**12**
Recovery (wt %)	78	74	68	71

The original and irradiated mixtures were then analyzed by high temperature simulated distillation (HTSD) to obtain the boiling point distributions shown in Figure 3. The boiling points of sample components are shown on the y-axis while the compound number (as defined in Figure 2) is given on the right side of the graph. The x-axis shows the proportion of the sample (weight %) that has evaporated at the corresponding (simulated) temperature on the y-axis. The graph in Figure 3 has a "terraced" profile where each plateau corresponds to the boiling point of the model compound or photooxidized product. The identities of compounds giving rise to these features were verified by GC×GC-TOF-MS data. Analysis of Figure 3 shows that two chemically pure photooxidation products, **X** and **Y**, having boiling points of 350 and 460 °C, respectively, have been generated. After 12 days of irradiation, products **X** and **Y** are seen to respectively constitute *ca.* 14 and 19 weight % of the sample. Within this sample, there also appears to be a complex mixture of photooxidation products having a boiling range of 460–750 °C, which constitutes the least volatile 10 weight %. For comparison, the original and control mixtures are seen to contain only 2–3 weight % of impurities in this boiling range. Taken together, *ca.* 40 weight % of the 12-day-irradiated mixture can be attributed to photooxidation products. Comparison of HTSD data for original and control samples also shows that approximately 15 weight % was lost due to evaporation incurred during extraction of the control while Table 3 shows that 22 weight % of the control was not recovered, indicating an unaccountable loss of 7 weight %.

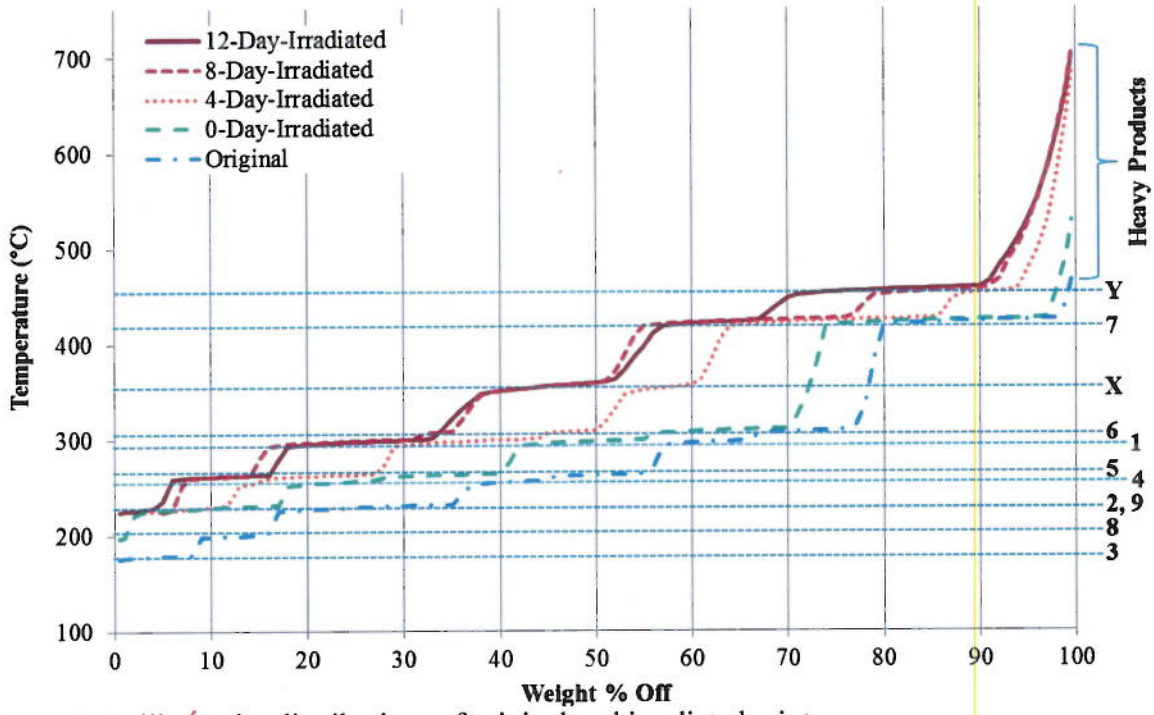

Figure 3. Boiling point distributions of original and irradiated mixtures

The mixtures were then analyzed by $^{13}C\{^{1}H\}$ NMR spectroscopy. The signals were integrated over the regions corresponding to the best-resolved signal from each compound present in the original mixture (shown in Table 2). The integrated intensities of these signals relative to the HMDSO signal were recorded. Since the NMR signal intensities obtained from a particular sample were dependent on the relative masses of analyte (m_A) and HMDSO (m_H) used, and in order to account for differences in mass recovery (m_R / m_I) following irradiation and extraction procedures, the integrated ^{13}C signal intensities (I) were converted to the corresponding normalized intensities (I_N), shown in Table 4, via the relationship:

$$I_N = (I \times m_R \times m_H \times 100.0\ mg) / (m_I \times m_A \times 40.0\ mg)$$

Table 4. Normalized ^{13}C signal intensities for compounds in original and irradiated mixtures

Compound		Normalized ^{13}C Signal Intensity, I_N				
		Original Mixture	Irradiation Time			
#	Name		0 d	4 d	8 d	12 d
1	Dibenzothiophene	9.07	9.10	9.09	9.11	9.11
2	Cyclohexylbenzene	4.33	2.53	1.58	0.19	0.52
3	*trans*-Decalin	9.99	0.00	0.00	0.00	0.00
4	1-Ethyl-2-methylindole	3.27	3.26	1.51	1.06	0.00
5	1-Phenyloctane	3.70	3.42	2.98	2.07	2.30
6	Benzyl sulfide	8.00	8.01	3.89	2.59	0.97
7	*n*-Dodecyl sulfide	8.98	8.92	6.11	5.25	3.28
8	Tetralin	7.83	1.77	0.00	0.00	0.00
9	1-Methylnaphthalene	3.80	2.63	1.75	0.49	0.78

Intensities are reported relative to the HMDSO signal set to 100.00. Intensities caused by noise are set to 0.00.

The difference between the normalized ^{13}C NMR signal intensities for a compound in the original (I_N^o) and irradiated (I_N^i) mixtures (from Table 4) was then used to calculate the percent loss (L) due to irradiation and extraction processes. Losses plotted in Figure 4 were calculated using:

$$L = [(I_N^o - I_N^i) / I_N^o] \times 100\ \%$$

Figure 4 illustrates, compound loss percentages versus their boiling points (listed in Table 1) to enable visual comparison of the independent effects of evaporation and photooxidation.

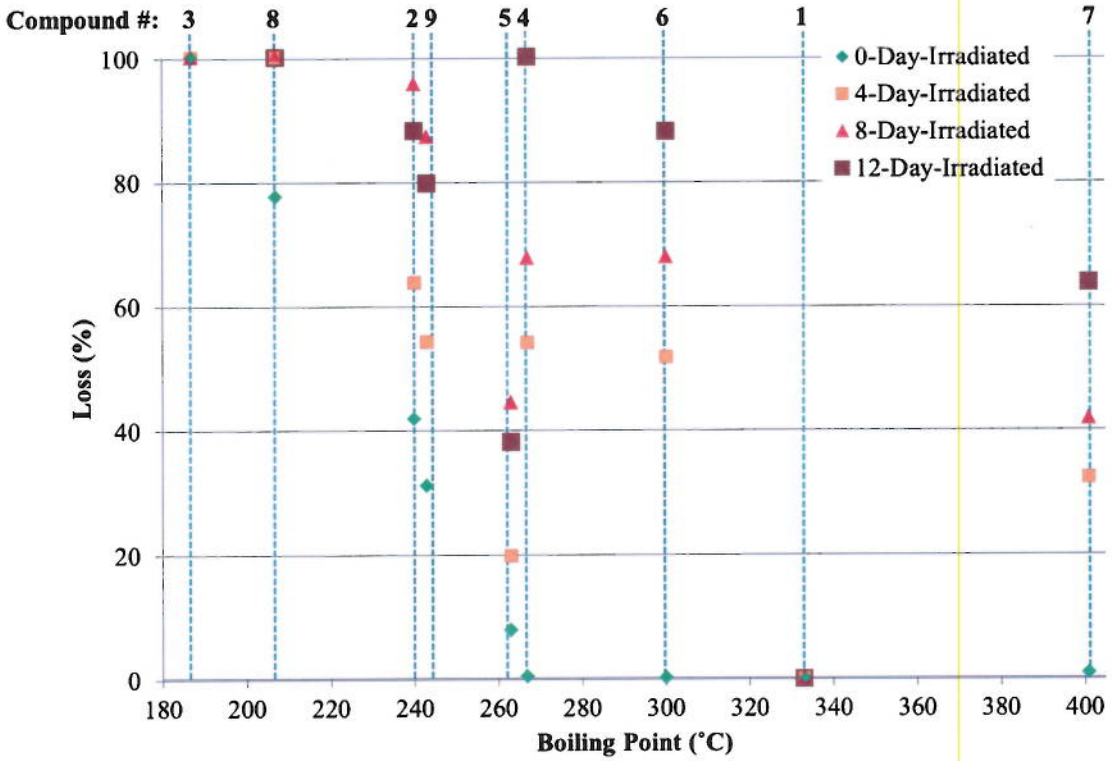

Figure 4. Compound loss versus boiling point at different irradiation times

Loss differences between the control (0-day-irradiated) mixtures and each of the 4-, 8- and 12-day-irradiated mixtures, depicted in Figure 4, are attributable to photo-conversion. Thus, in order to compare photooxidative compound losses, photo-conversion (PC) values were calculated as the loss difference between irradiated (L^i) and control (L^0) mixtures relative to the proportion not lost during the extraction procedure (i.e., remaining in the control; $100 - L^0$). PC values, plotted in Figure 5 against boiling points, were calculated via the relationship:

$$PC = [(L^i - L^0) / (100 - L^0)] \times 100\ \%$$

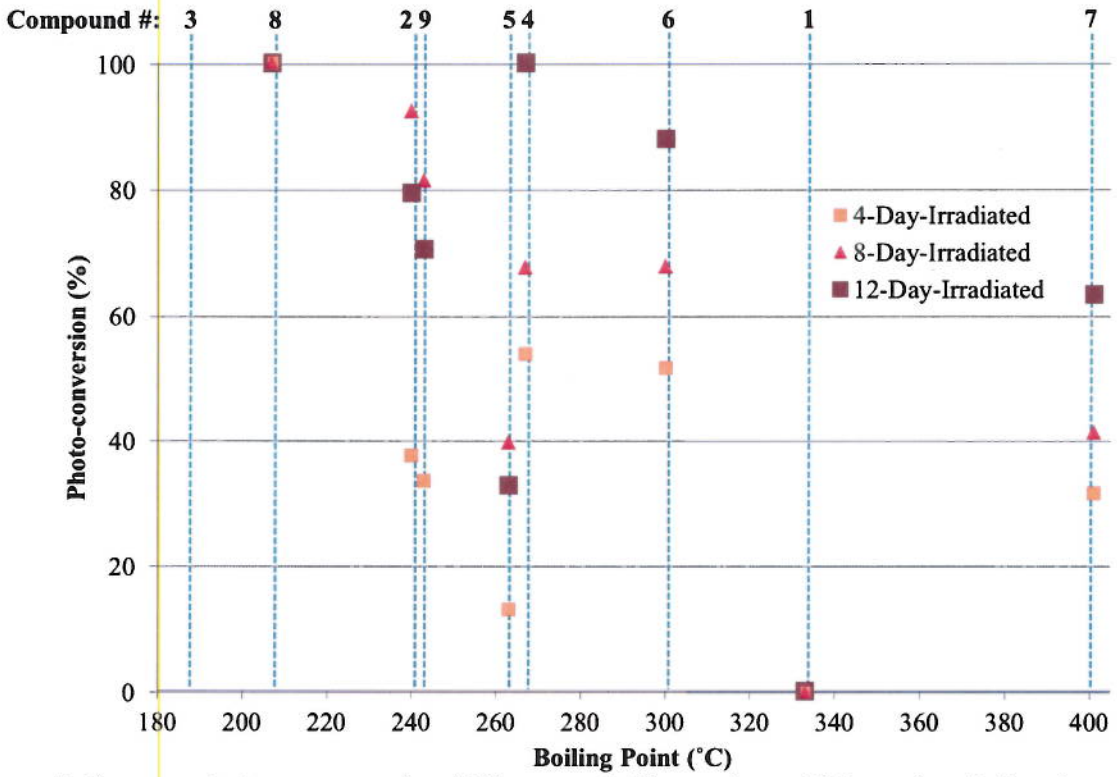

Figure 5. Compound photo-conversion (PC) versus boiling point at different irradiation times

Analysis of the control data for the 0-day-irradiated mixture in Figures 4 shows that varying amounts of the most volatile components (**3** > **8** > **2** ~ **9** > **5**) are lost following the extraction procedure, and the trend reflects their boiling points. Consequently, this loss is likely due to evaporation incurred during this procedure. No evidence of the most volatile compound, *trans*-decalin (**3**; BP = 187 °C), could be found from NMR spectra of either the control or irradiated mixtures, and thus no PC could be calculated for this compound. In addition to evaporation, it may be anticipated that partitioning of compounds into the aqueous phase during extraction could also account for some loss. However, such partitioning did not appear to be significant as the control mixture suffered little or no loss of sulfur- and nitrogen-containing compounds (**1**, **4**, **6** and **7**), which presumably have higher water-solubilities owing to their hydrogen-bond acceptor functionality. While the observation that compounds **2**, **5**, and **9** each appeared to suffer slightly greater photo-conversions after 8 days of irradiation than they did after 12 days (perhaps reflecting some experimental inconsistency), the average photo-conversion of all compounds after 8 days of irradiation (61 %) was found to be less than it was after 12 days (67 %).

FTIR spectra of control and irradiated mixtures, shown in Figure 6, were obtained to determine changes in the abundance of oxygen-containing carbonyl (C=O stretch at 1708 cm^{-1}) and sulfoxide (S=O stretch at 1027 cm^{-1}) functional groups.

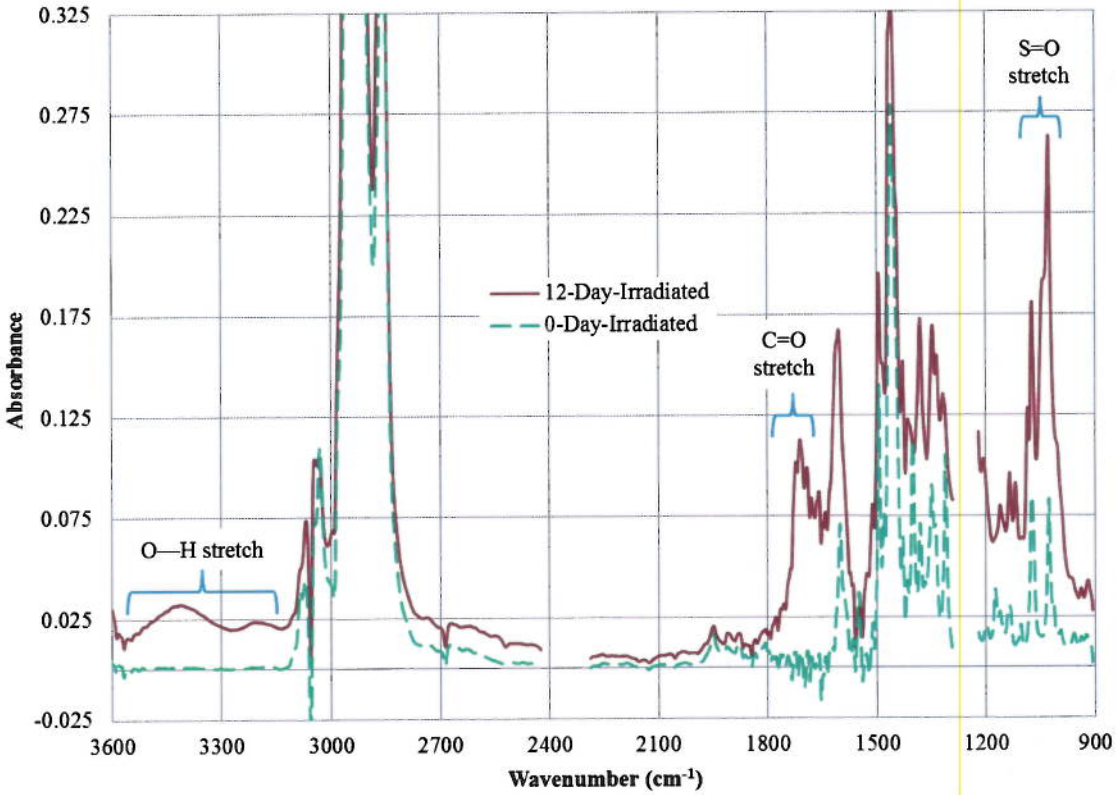

Figure 6. FTIR spectra of control and 12-day-irradiated model mixtures

Variously concentrated cyclohexanebutyric acid (CHBA) standards in toluene (0, 10, 50, 100 and 290 mM) were analyzed by FTIR spectroscopy in CH_2Cl_2 solution to determine the relationship between C=O signal strength and concentration. The resulting spectra were integrated over the carbonyl region between 1785–1650 cm^{-1}, which is inclusive of signals arising from carboxylic acids, esters, ketones, aldehydes and amides. A calibration curve of known CHBA concentration versus normalized integrated absorbance revealed a linear relationship ($R^2 = 0.9999$). Similarly, a calibration curve for S=O signals was attempted using a series of dimethyl sulfoxide (DMSO) standards, but was considered not to be adequate due to interference from overlapping signals arising from C—O stretching and C—C—X bending modes. The areas of the carbonyl bands were compared to the standard curve and converted to the contents of C present as C=O using the carbon contents given in Table 5. The content of C present as C=O in the model oil samples was found to increase with photooxidation, and is plotted against irradiation time in Figure 7.

Table 5. Elemental compositions of model mixtures

Element	Content (wt %)				
	Original Mixture	Irradiation Time			
		0 d	4 d	8 d	12 d
C	83.7	81.9	76.9	76.2	76.9
H	10.0	9.0	9.2	9.2	9.6
N	0.8	1.0	1.1	1.1	1.1
S	5.2	7.3	8.4	9.0	7.7
O	0.3	0.8	4.4	4.5	4.7

Oxygen content in original and control mixtures may reflect experimental error and/or impurities present (see "Purity" column in Table 1).

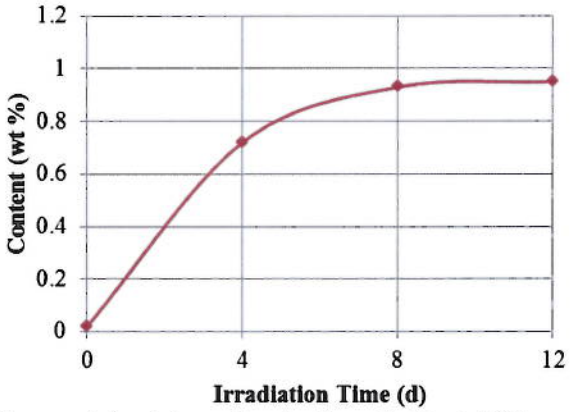

Figure 7. Proportions of the model mixture due to C as C=O at different irradiation times

Two-dimensional gas chromatography (GC×GC) of the original and irradiated mixtures revealed signals due to the presence of new photooxidation products, **A–D**, in Figure 8. The identities of these and other signals (**E–O**, not depicted for clarity) were determined by analyzing the GC×GC-separated sample components by time-of-flight mass spectrometry (TOF-MS) and matching the resulting isotope distribution patterns with those available in a database. With the exception of compound **D**, products **A–O** were identified, and their chemical structures are given in Figure 9.

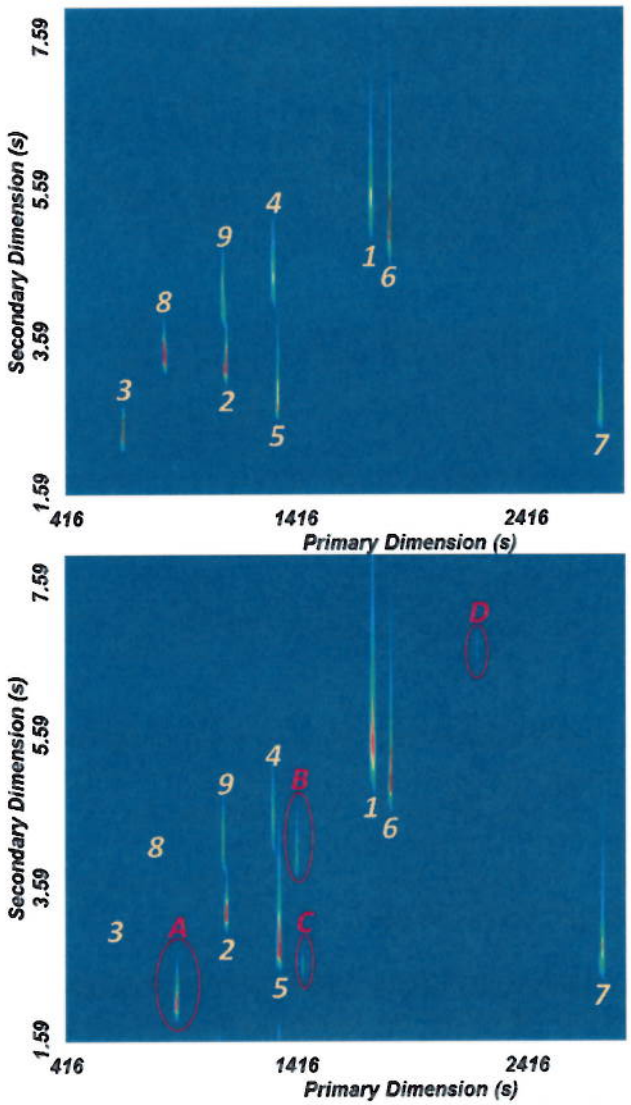

Figure 8. 2D gas chromatographs of original (left) and 4-day-irradiated (right) mixtures

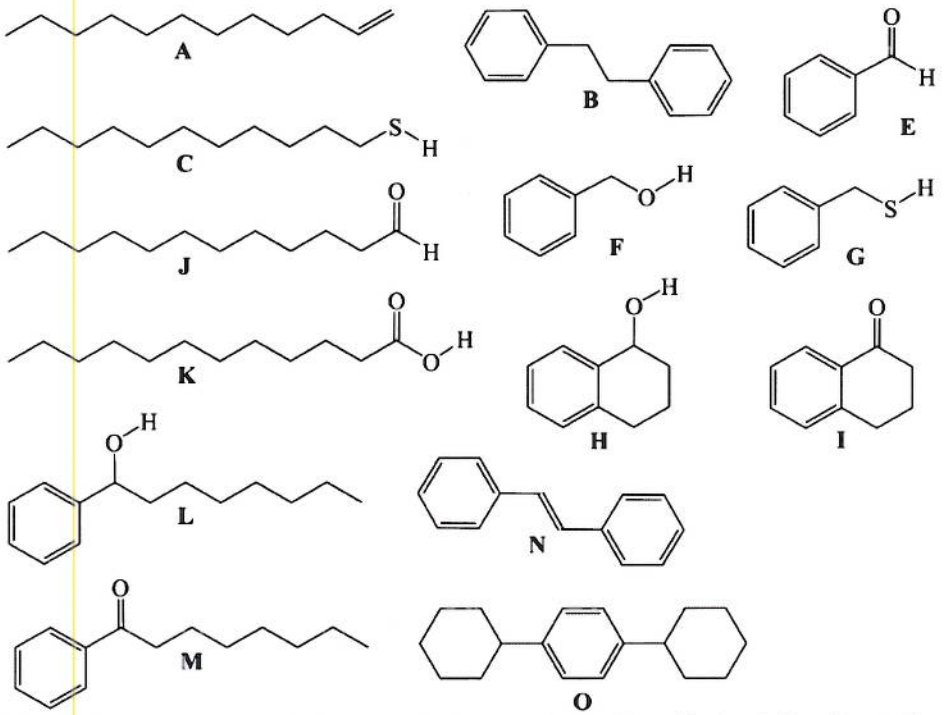

Figure 9. Molecular structures of photooxidation products identified within the 4-day-irradiated mixture where the compound names are: **A** = 1-dodecene, **B** = bibenzyl, **C** = 1-dodecanethiol, **D** = unidentifiable ($[M]^+$ = 182 m/z), **E** = benzaldehyde, **F** = benzenemethanol, **G** = benzenemethanethiol, **H** = 1,2,3,4-tetrahydro-1-naphthalenol, **I** = 1,2,3,4-tetrahydronaphthalen-1-one, **J** = dodecanal, **K** = dodecanoic acid, **L** = 1-phenyl-1-octanol, **M** = 1-phenyl-1-octanone, **N** = stilbene, **O** = *para*-dicyclohexylbenzene.

3.2 Photooxidation of Diluted Bitumen (DB) and its Subfractions

The separation of DB (BP > 204 °C) into saturates, aromatics, resins and asphaltenes (SARA) subfractions yielded the following mass proportions: 22.4 % saturates, 41.9 % aromatics, 18.6 % resins, and 17.1 % asphaltenes (*n*-pentane-insoluble). The original DB, and its saturates and aromatics subfractions were irradiated for 8-day periods then characterized in a manner analogous to that of the model mixtures. Irradiation of the moderately viscous, opaque, black DB for 8 days resulted in its conversion to a solid crust on the water's surface. On the other hand, the less viscous, transparent, colourless DB-saturates subfraction underwent little visible change apart from becoming mildly opaque and taking on a very faint yellow discoloration. However, during irradiation, the orange-coloured, transparent, moderately viscous DB-aromatics subfraction formed a dark brown-coloured, initially buoyant crust. However, upon gentle agitation of the vial after its removal from the cooling bath, the crust sank to the bottom of the water column indicating that its density was greater than that of the water. Conversely, agitation of the irradiated sample of DB on water did not cause it to sink, although the majority of the crust was submerged just below the water's surface.

After extraction and isolation, the mass recovery was determined as shown in Table 6. Irradiation of original DB for 8 days resulted in mass loss of 3 weight %. Similarly, the DB saturates and aromatics subfractions also experienced low mass losses due to photooxidation.

Table 6. Recoveries of DB and its subfractions after irradiation and/or extraction

Subfraction	Original		Saturates		Aromatics	
Irradiation Time (d)	0	8	0	8	0	8
Recovery (wt %)	87	84	87	85	97	95

ND = Not determined.

Figure 10 shows the HTSD curves of the original DB and its subfractions, as well as those of their irradiated products. There is a significant change in the shape of the curve of the original DB before and after 8 days of irradiation. As demonstrated for the model compound study, loss of the low boiling ("light ends") fraction of the oil is expected during the isolation procedure. To determine the extent of loss, the original DB was subjected to the rotary evaporation method used within the extraction protocol to create the "DB > 200 °C" sample. Comparison of the "DB-Original," "DB > 200 °C," and "DB-Irradiated" boiling point distribution curves shows that significant loss of light ends from the original oil is mainly due to evaporation incurred during this step. As indicated by the recovery data presented in Table 6, similar loss was observed for the saturates subfraction, while the aromatics subfraction had the highest recovery following the extraction procedure. The effects of these losses on the boiling point curves for the samples can also be observed in Figure 10.

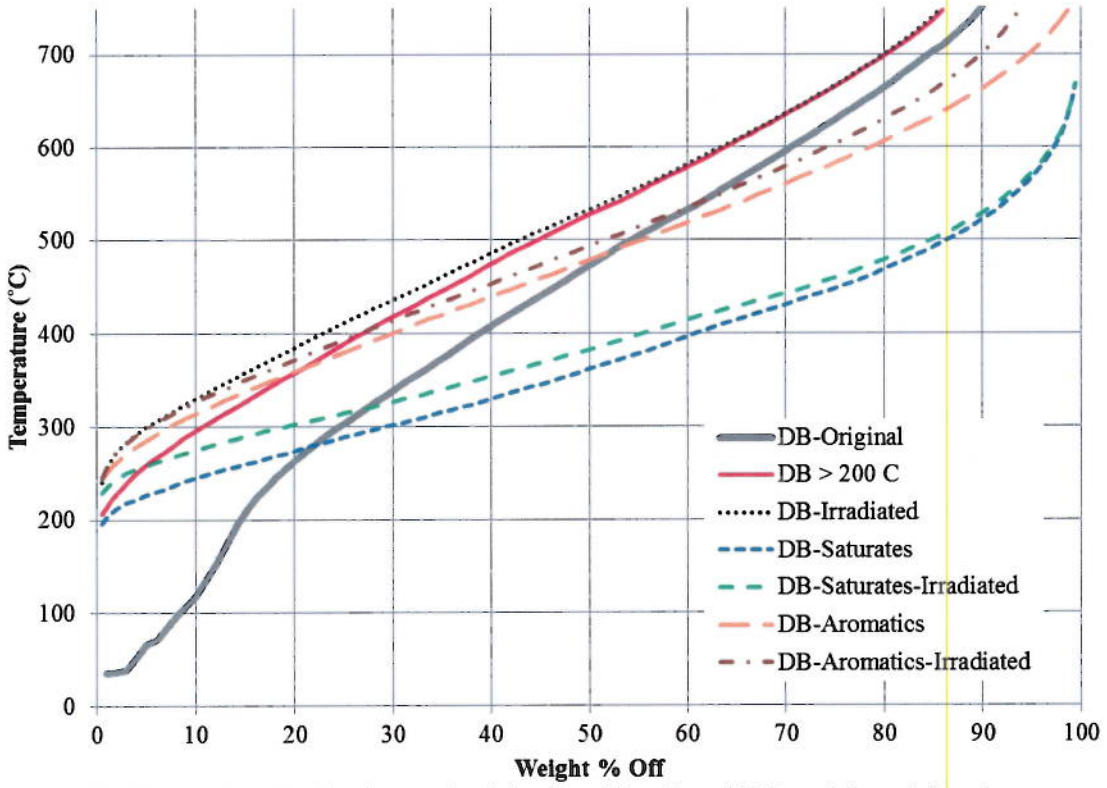

Figure 10. Boiling point distributions of original and irradiated DB and its subfractions

Elemental compositions of the original and irradiated DB and subfractions are shown in Table 7. By comparing the compositions of the original DB to its saturates and aromatics fractions, the saturates are seen to have the highest hydrogen content and the lowest sulfur and

nitrogen contents of the three samples. For all three samples, oxygen content increased with irradiation, particularly for the DB and aromatics samples.

Table 7. Elemental contents of original and irradiated samples of DB and its subfractions

Element	Content (wt %)						
	DB			DB-Saturates		DB-Aromatics	
	Original	> 200 °C	Irradiated	Original	Irradiated	Original	Irradiated
C	83.8	83.7	82.9	85.6	85.3	84.4	83.3
H	11.0	11.3	10.8	14.2	14.3	10.8	10.7
N	0.4	0.4	0.4	0.1	0.1	0.1	0.1
S	4.3	4.1	4.4	0.0	0.0	4.3	4.4
O	0.5	0.5	1.5	0.1	0.3	0.4	1.5

FTIR spectra of DB > 200 °C and irradiated DB, shown in Figure 11, illustrate the expected increases in C=O and S=O signal intensities observed in the model mixtures after irradiation. However, comparison of these spectra with those of the model mixture reveals that the intensities of these signals were substantially lower. In particular, the intensity of the O—H stretching signal in Figure 10 was not found to increase after irradiation of the DB.

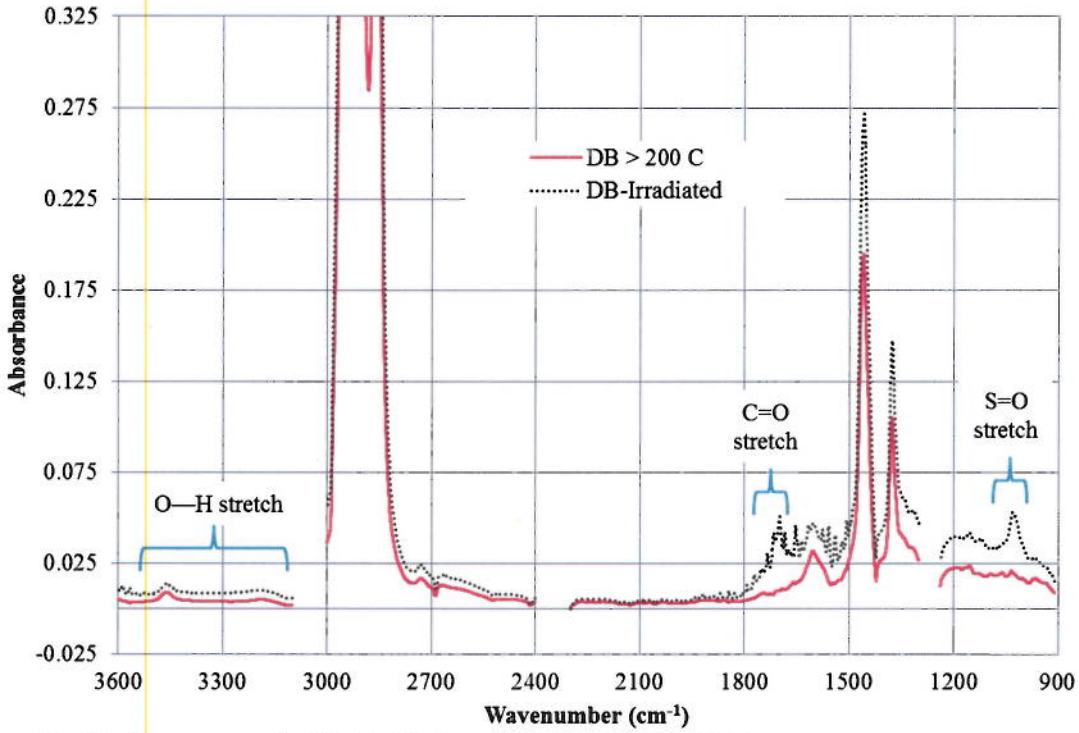

Figure 11. FTIR spectra of DB > 200 °C and 8-day-irradiated DB

The elemental and FTIR data, together with $^{13}C\{^{1}H\}$ and ^{1}H NMR analyses, enabled quantification of the different carbon types shown in Table 8. Comparing carbon type data of original DB with that of DB > 200 °C shows a greater aromatic carbon content in the latter at the expense of paraffinic carbon. This trend is expected because a substantial proportion of the

lightest fractions lost are alkanes. The most significant changes that occurred after irradiation were slight increases in the contents of olefinic and carbonyl carbon relative to the DB > 200 °C sample. In the case of the saturates subfraction, the slight increase of oxygen content was not detected as carbonyl carbon. Otherwise, the compositions of the saturates samples before and after irradiation were very similar. The most significant changes due to irradiation were found for the aromatics sample. The content of aromatic carbon increased predominantly with the loss of cycloparaffinic carbon. There were also slight increases in both olefinic and carbonyl carbon types with irradiation.

Table 8. Carbon type quantification of original and irradiated DB and its subfractions

Carbon Type	Carbon Content (mol %)						
	DB			DB-Saturates		DB-Aromatics	
	Original	> 200C	Irrad.	Original	Irrad.	Original	Irrad.
Aromatic	24.1	28.2	27.4	1.8	1.8	30.7	34.5
Cycloparaffinic	31.2	32.2	32.0	54.0	54.0	31.4	28.9
Branched Paraffinic	9.8	7.3	7.7	15.9	15.9	5.0	5.8
Chain Paraffinic (C1+)	34.7	32.1	32.1	28.1	28.1	32.7	30.3
Olefinic	0.2	0.2	0.6	0.3	0.3	0.1	0.2
C=O	0.0	0.0	0.2	0.0	0.0	0.1	0.3

4 Discussion

In this work, the relative photooxidation susceptibility and fate of chemically distinct components of petroleum were evaluated. When crudes spill on water, the susceptibility of the oil to photooxidation depends upon both physical factors (oil thickness and transparency, hours per day of exposure to sunlight, strength of sunlight) and chemical factors (oil composition including types of hydrocarbons and heteroatom content). The light ends of spilled crude oils (consisting of hydrocarbons with carbon number < 15) will be removed relatively quickly after an oil spill due to evaporation and biodegradation processes. To gain more information on factors influencing the reactivity of the more persistent petroleum species to sunlight, both model oil and diluted bitumen (DB) were studied. For the model oil, a series of chemical compounds representing common petroleum hydrocarbon types was selected and blended to form a model mixture. The mixture was then applied to the surface of water and irradiated. After irradiation, the organic-extractable fraction was isolated and characterized to determine the relative photooxidation susceptibilities of its components. The identities of major photooxidation products were also determined. This approach was then applied to DB as well as saturates and aromatics subfractions.

4.1 Photooxidation of Model Mixture

The model oil consisted of a mixture of aromatics [dibenzothiophene (**1**), cyclohexylbenzene (**2**), 1-ethyl-2-methylindole (**4**), 1-phenyloctane (**5**), benzyl sulfide (**6**), and 1-methylnaphthalene (**9**)], a hydroaromatic [tetralin (**8**)], a cycloalkane [*trans*-decalin (**3**)] and an alkyl sulfide [*n*-dodecyl sulfide (**7**)]. The photo-conversion (PC) results in Figure 4 show that model compound photooxidation susceptibility decreases approximately in the order: tetralin > cyclohexylbenzene ~ 1-ethyl-2-methylindole ~ benzyl sulfide ~ 1-methylnaphthalene > 1-phenyloctane ~ *n*-dodecyl sulfide > dibenzothiophene. So, dibenzothiophene (**1**) was found to be

the least reactive component. By comparing the relative reactivity of compounds **2** and **5**, it can be inferred that cycloalkyl substituents on aromatic rings are more reactive than linear alkyl groups, consistent with the greater reactivity of methine (R_3CH) groups (as in **2**) to free radical-initiating hydrogen atom abstraction by photo-generated hydroxyl (HO•) radicals. By observing the relative reactivity of sulfur-containing compounds **1**, **6** and **7**, it can be inferred that the aromatic sulfur species, dibenzothiophene (**1**), is much less reactive than either of the sulfidic compounds, although the presence of aromatic groups in compound **6** makes it somewhat more reactive than dialkyl sulfide, **7**. The *trans*-decalin (**3**) could not be compared to the other compounds because its boiling point was sufficiently low that it was completely lost during the isolation procedure. However, analyses of the reactivity of the saturates subfraction of DB will provide insight into the reactivity of cycloalkanes (discussed in **4.2**).

A comparison of the elemental contents of the model oil in Table 5 to that of the DB in Table 7 shows that their elemental compositions were similar. With loss of the most volatile components, the model oil had become enriched in N, S and O contents. This observation was consistent with ^{13}C NMR spectroscopic data indicating that the extraction process resulted in evaporative loss of the more volatile compounds, **2**, **3**, **8** and **9**, none of which contain heteroatoms. As expected, irradiation of the original mixture resulted in further changes in elemental composition, with the most obvious difference being the order of magnitude increase in O content relative to the original mixture. The increase in sulfur content up to 8 days followed by its decrease after 12 days suggests the loss of sulfur-enriched compounds during that time period. This decrease, considered in light of FTIR evidence for the increased content of S present as S=O, appears to reflect loss of S content, presumably in the form of volatile and/or water-soluble organic and inorganic (i.e., H_2SO_4) sulfur compounds (Bobinger, 2009). Analysis of the mixtures' FTIR spectra, depicted in Figure 6, shows that signals corresponding to the presence of oxygen-containing functional groups, specifically hydroxyls (O–H stretch, centered at 3416 cm^{-1}), carbonyls (C=O stretch, centered at 1705 cm^{-1}) and sulfoxides (S=O stretch, centered at 1027 cm^{-1}), increase in intensity upon irradiation of the original mixture.

Analysis of the high-temperature simulated distillation (HTSD) data shown in Figure 3 shows that irradiation of the original mixture on water increases the heavy fraction boiling > 400 °C. Although this feature is certainly attributable in part to evaporation of lighter components, it is clear that heavier unidentified products boiling between *ca.* 401–700°C, are also generated, presumably as a result of photo-induced condensation reactions between aromatic components. Although it is well understood that photooxidation reactions tend to convert larger molecules into smaller, more readily decomposable ones, photo-induced condensations of aromatic components have also been found to increase the proportion of the heavier fraction (Feng et al., 2012).

Figure 3 shows two prominent, unidentified photooxidation products, labelled as **X** and **Y**, having well-defined boiling points of *ca.* 350 and 460 °C, respectively, which are evident only in boiling point distributions of the irradiated samples. Although the identities of these products could not be verified, **X** appears to be a nitrogen-containing compound resulting from decomposition of component **4**. Support for this interpretation can be seen in the boiling point distributions in Figure 3 as the observed decrease in the proportion of **4** approximates the observed increase in the proportion of **X**. Further support can be gathered from GC×GC-TOF-MS data in Figure 8, which exhibits a signal for an unidentified photooxidation product, **D** with m/z = 182, consistent with a single, nitrogen-containing species resulting from photo-conversion of **4**. The identity of product **Y** is postulated as either dodecyl sulfoxide ($C_{24}H_{50}SO$) or the

corresponding sulfone ($C_{24}H_{50}SO_2$) resulting from oxidation of **7** on the grounds that the proportion of **7** decreases to the approximate extent that **Y** increases. The fact that such a species was not observed from GC×GC-TOF-MS data is consistent with the introduction of oxygen into **7**, which would increase its boiling point above 400 °C, just beyond that observable by this technique.

Two-dimensional gas chromatographs of the original and 4-day irradiated mixtures, shown in Figure 8, reveal the generation of several other photooxidation products in the latter. Comparisons of the retention times and mass spectral data for these eluents with a database reveal the identities of 14 photooxidation products illustrated in Figure 9. From these data, and in light of the points discussed above, it can be reasonably surmised that photooxidation of dibenzothiophene (**1**) did not occur to any appreciable extent, while cyclohexylbenzene (**2**) produced compound **O**. The volatile component, *trans*-decalin (**3**) was completely removed by evaporation and extraction steps and thus determination of its photooxidation products was not possible. The nitrogen-based component, 1-ethyl-2-methylindole (**4**) was converted into an unidentified N-containing product, **D** (presumably = **X** in Figure 3), based on its even-numbered mass-to-charge ratio. Photooxidation of 1-phenyloctane (**5**) generated products **L** and **M**, while benzyl sulfide (**6**) was converted into products **B**, **E**, **F**, **G**, and **N**. Photooxidation of *n*-dodecyl sulfide (**7**) gave products **A**, **C**, **J** and **K**, while tetralin (**8**) was converted into products **H** and **I**.

4.2 Photooxidation of Diluted Bitumen (DB) and its Subfractions

Unlike the model mixture, irradiation of DB for 8 days resulted in only very slight changes to its elemental composition, as can be seen in Table 7. This may be expected given the complexity of hydrocarbons present in the oil. However, as well, the physical accessibility of photons into the DB would be lower than that of the model oil, which was transparent. For instance, during irradiation of the model mixture on water, the bottom of the glass vial could be seen though the slick, while in the case of DB it could not. In contrast, original DB absorbed visible light (constituting the majority of photons emitted from the light source) much more strongly than the initially transparent model mixture. The higher opacity of DB is attributable to its high contents of resins (18.6 weight %) and asphaltenes (17.1 weight %) which contain larger, more strongly absorbing molecules than those comprising the model mixture. It may be inferred that strong visible light absorbance by the uppermost surface of the slick shielded the underlying bulk of the DB from a strong flux of photons, thereby inhibiting its photooxidation when compared to the model mixture. Evaporation of the lightest components of DB exacerbates this effect by increasing the slick's viscosity. The gradual formation of a semi-solid mat of oil afloat at the water's surface would impede mass transport of oxygen and other reactive oxygen species responsible for initiating radical photooxidation reactions (Nair, 1993).

The observation that the DB saturates subfraction also underwent little change in terms of its elemental composition following irradiation is not surprising despite its transparency, and may be attributed instead to the reported resistance of saturated hydrocarbons against photooxidation (Garrett, 1998). The carbon type analyses of saturates samples, presented in Table 8, show that over half of the carbon in the samples is present as cycloalkanes. Consequently, that there was no difference in carbon type composition after irradiation demonstrates that cycloalkanes have low photooxidation susceptibility, supplementing the results of the model oil. In comparison, irradiation of the DB aromatics subfraction complimented the reactivity of hydroaromatics observed for the model oil. Table 8 shows that content of cycloalkane carbon decreased with an increase in aromatic carbon content. As some of the

cycloalkane carbon would be contained within hydroaromatic structures, they appear to be removed leaving the remaining oil more aromatic.

The carbon type data in Table 8 show that irradiation of DB resulted in a slight loss of aromatic carbon content relative to that of DB > 200 °C, with small increases in the proportions of branched paraffinic and olefinic carbon contents. This change reflects the occurrence of photooxidative ring-opening of aromatic components akin to that depicted in Figure 1. Concomitant production of olefins is certainly also expected as compounds **6** and **7** were shown to undergo photo-conversion to yield olefinic products **N** and **A**, respectively. Similarly, a slight increase in olefinic and branched paraffinic carbon was also detected in the irradiated aromatics subfraction.

Finally, FTIR spectra of DB > 200 °C and 8-day-irradiated DB samples in Figure 11 qualitatively illustrate the results reflected quantitatively in the elemental and NMR carbon type data for the original and irradiated DB and subfractions. As expected, there are noticeable increases in the absorbance intensities of C=O and S=O stretching signals within the spectra of irradiated DB relative to the non-irradiated oil. However, these intensity increases are much less pronounced than those observed within the spectra of the model mixtures shown in Figure 6. The apparent lack of increase in O—H band intensity in the irradiated DB sample likely reflects its reduced photooxidation susceptibility compared to that of the model oil. The smaller extinction coefficient for O—H absorbance relative to those of C=O and S=O groups renders small changes in hydroxyl group concentration unnoticeable; the presence of a small signal in these spectra may only be due to residual water content of the sample.

5 Conclusion

A study of photooxidation was conducted on model oil consisting of hydrocarbon compounds representing those found in petroleum. From this study, it can be seen that irradiation timescales equivalent to 2 to 6 months of exposure on Canada's west coast can give rise to high photo-conversion of oil components, although this does not necessarily indicate that photooxidation will ultimately lead to complete photo-conversion of oil into CO_2 and water. The model compound results clearly illustrated that there are hydrocarbon types in petroleum that are resistant to photooxidation on this timescale. Certainly, the observation of decades-old, persistent oil on Canada's coastlines speaks to the limited efficacy of photooxidation for removing petroleum from the environment. Beyond chemical reactivity, physical effects such as the inability for light to access hydrocarbons below the oil surface also interfere. In this study, the observation of minimal photo-chemical reactivity of DB was attributable to its strong photo-absorbing properties, which prevent light from penetrating the uppermost surface of the oil. As well, evaporation of the lightest components of DB exacerbates this effect by increasing the slick's viscosity. Future research will involve analyses of products generated in both organic and aqueous phases to more fully understand the fate of the photooxidized products. Work will also explore the possibility of increasing both the rates and extent of petroleum photooxidation with the application of photocatalytic additives.

6 Acknowledgements

The authors would like to thank the Analytical Laboratory and Environmental Impacts staff at CanmetENERGY – Devon for their assistance and performance of chemical analyses. This work received funding support from both the World Class Tanker Safety Program and the

government of Canada's Interdepartmental Program on Energy Research and Development (PERD).

7 References

Bobinger, S. and T.J. Anderson, "Photooxidation Products of Polycyclic Aromatic Compounds Containing Sulfur", *Environ. Sci. Technol.*, 43:8119-8125, 2009.

Bobra, M. and E.J. Tennyson, "Photooxidation of Petroleum", *Proceedings of the Twelfth Arctic Marine Oilspill Program Technical Seminar*, Environment Canada, Ottawa, ON, 1:129-147, 1989.

Committee on Marine Transportation of Heavy Oils, Marine Board, Commission on Engineering and Technical Systems, and National Research Council, "Spills of Non-Floating Oils: Risk and Response", Report, National Academy of Sciences, Washington, DC, 75 p., 1999.

Committee on the Effects of Diluted Bitumen on the Environment, Board on Chemical Sciences and Technology, Division on Earth and Life Studies, and National Academies of Sciences, Engineering, and Medicine, *Spills of Diluted Bitumen from Pipelines: A Comparative Study of Environmental Fate, Effects, and Response*, Report, National Academy of Sciences, Washington, DC, 145 p., 2016.

Díez, S., E. Jover, J.M. Bayona, and J. Albaigés, "Prestige Oil Spill. III. Fate of a Heavy Oil in the Marine Environment", *Environ. Sci. Technol.*, 41:3075-3082, 2007.

Dutta, T.K. and S. Harayama, "Fate of Crude Oil by the Combination of Photooxidation and Biodegradation", *Environ. Sci. Technol.*, 34:1500-1505, 2000.

Ehrhardt, M.G., M.C. Bícego, and R.R. Weber, "Photo-oxidation of 1-Methylnaphthalene Dissolved in Seawater and Exposed to Sunlight under Quasi-environmental Conditions", *J. Photochem. Photobiol. A: Chem.*, 108:253-259, 1997.

Environment Canada, Fisheries and Oceans Canada, and Natural Resources Canada, *Properties, Composition and Marine Spill Behaviour, Fate and Transport of Two Diluted Bitumen Products from the Canadian Oil Sands*, Federal Government Technical Report, Environment Canada, Ottawa, ON, 85 p., 2013.

Feng, Y.-L., J.P. Nandy, Y. Hou, F. Breton, B. Lau, J. Zhang, and J. Zhu, "UV Light Induced Transformation of 1-Methylnaphthalene in the Presence of Air and Its Implications for Contaminants Research", *J. Environ. Prot.*, 3:1519-1531, 2012.

Forstner, H.J.L., R.C. Flagan, J.H. Seinfeld, "Secondary Organic Aerosol from the Photooxidation of Aromatic Hydrocarbons: Molecular Composition", *Environ. Sci. Technol.*, 31:1345-1358, 1997.

Garrett, R.M., I.J. Pickering, C.E. Haith, and R.C. Prince, "Photooxidation of Crude Oils", *Environ. Sci. Technol.* 32:3719-3723, 1998.

Gong, Y., X. Zhao, Z. Cai, S.E. O'Reilly, X. Hao, and D. Zhao, "A Review of Oil, Dispersed Oil and Sediment Interactions in the Aquatic Environment: Influence on the Fate, Transport and Remediation of Oil Spills", *Mar. Pollut. Bull.*, 79:16-33, 2014.

Hounjet, L.J. and H.D. Dettman, "Impacts of Pretreatment on the Properties and Behaviour of Diluted Bitumen in Water", *Proceedings of the Thirty-ninth AMOP Technical Seminar*, Environment and Climate Change Canada, Ottawa, ON, 1:472-493, 2016.

Japanwala, S., K.H. Chung, H.D. Dettman, and M.R. Gray "Quality of Distillates from Repeated Recycle of Residue", *Energy Fuels*, 16:477-484, 2002.

King, S.M., P.A. Leaf, A.C. Olson, P.Z. Ray, and M.A. Tarr, "Photolytic and Photocatalytic Degradation of Surface Oil from the Deepwater Horizon Spill", *Chemosphere*, 95:415-422, 2014.

King, T.L., B. Robinson, C. McIntyre, P. Toole, S. Ryan, F. Saleh, M.C. Boufadel, and K. Lee, "Fate of Surface Spills of Cold Lake Blend Diluted Bitumen Treated with Dispersant and Mineral Fines in a Wave Tank", *Environ. Eng. Sci.*, 32:250-261, 2015.

Lee, K., M. Boufadel, B. Chen, J. Foght, P. Hodson, S. Swanson, and A. Venosa, *Behaviour and Environmental Impacts of Crude Oil Released into Aqueous Environments*, Expert Panel Report, Royal Society of Canada, Ottawa, ON, 460 p., 2015.

Lee, R.F. "Photo-oxidation and Photo-toxicity of Crude and Refined Oils", *Spill Sci. Technol. Bull.*, 8:157-162, 2003.

Maki, H., T. Sasaki, and S. Harayama, "Photo-oxidation of Biodegraded Crude Oil and Toxicity of the Photo-oxidized Products", *Chemosphere*, 44:1145-1151, 2001.

Markusoff, J. (2017), *Does Spilled Pipeline Bitumen Sink or Float?* Retrieved January, 2017 from http://www.macleans.ca/society/does-spilled-pipeline-bitumen-sink-or-float

Minero, C., V. Maurino, and E. Pelizzetti, "Photocatalytic Transformations of Hydrocarbons at the Sea Water / Air Interface under Solar Radiation", *Mar. Chem.*, 58:361-372, 1997.

Nair, M., Z. Luo, and A. Heller, "Rates of Photocatalytic Oxidation of Crude Oil on Salt Water on Buoyant, Cenosphere-attached Titanium Dioxide", *Ind. Eng. Chem. Res.*, 32:2318-2323, 1993.

O'Laughlin, C., B.A. Law, V.S. Zions, T.L. King, B. Robinson, and Y. Wu, *The Dynamics of Diluted Bitumen Derived Oil-mineral Aggregates, Part I.*, Technical Report No. 3157, Fisheries and Oceans Canada, Dartmouth, NS, 44 p., 2016.

Sato, K., S. Hatakeyama, and T. Imamura, "Secondary Organic Aerosol Formation during the Photooxidation of Toluene: NO_x Dependence of Chemical Composition", *J. Phys. Chem. A*, 111: 9796-9808, 2007.

Shankar, R., W.J. Shim, J.G. An, and U.H. Yim, "A Practical Review on Photooxidation of Crude Oil: Laboratory Lamp Setup and Factors Affecting It", *Water Res.*, 68:304-315, 2015.

Solar Electricity Handbook (2017) Retrieved January, 2017 from http://solarelectricityhandbook.com/solar-irradiance.html

Solum, M.S., R.J., Pugmire, and D.M. Grant, "Carbon-13 Solid-State NMR of Argonne-Premium Coals", *Energy Fuels*, 3:187-193, 1989.

Witt O'Brien, Polaris Applied Sciences, and Western Canada Marine Response Corporation, *A Study of Fate and Behaviour of Diluted Bitumen Oils on Marine Waters: Dilbit Experiments*, Report, Gainford, AB, 67 p., 2013.

Yang, F., P. Tchoukov, H. Dettman, R.B. Teklebrhan, L. Liu, T. Dabros, J. Czarnecki, J. Masliyah, and Z. Xu, "Asphaltene Subfractions Responsible for Stabilizing Water-in-Crude Oil Emulsions. Part 2: Molecular Representations and Molecular Dynamics Simulations", *Energy Fuels*, 29:4783-4794, 2015.

Zhou, J., H. Dettman, and M. Bundred, "A Comparative Analysis of Environmental Behaviour of Diluted and Conventional Crudes", *Proceedings of the Thirty-Eighth AMOP Technical Seminar*, Environment Canada, Ottawa, ON, 1:495-516, 2015.